NANO LETTERS

pubs.acs.org/NanoLett Letter

Adsorption and Diffusion of Oxygen on Pure and Partially Oxidized Metal Surfaces in Ultrahigh Resolution

Krishan Kanhaiya and Hendrik Heinz*

Cite This: *Nano Lett.* 2022, 22, 5392−5400 Read Online

ABSTRACT: The interaction of gas molecules with metal and oxide surfaces plays a critical role in corrosion, catalysis, sensing, and heterogeneous materials. However, insights into the dynamics of O_2 from picoseconds to microseconds have remained unavailable to date. We obtained 3D potential energy surfaces for adsorption of O_2 on 11 common pristine and partially oxidized (hkl) surfaces of Ni and Al in picometer resolution and high accuracy of 0.1 kcal/mol, identified binding sites, and surface mobility from 25 to 300 °C. We explain relative oxidation rates and parameters for oxide growth. We employed over 150 000 molecular mechanics and molecular dynamics simulations with the interface force field (IFF) using structural data from X-ray diffraction (XRD) and low-energy electron diffraction (LEED). The methods reach 10 to 50 times higher accuracy than possible before and are suited to analyze gas interactions with metals up to the micrometer scale including defects and irregular nanostructures.

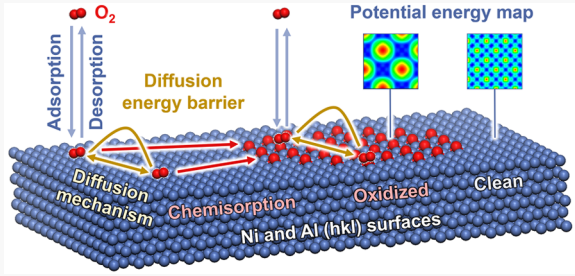

KEYWORDS: *metal-gas interfaces, adsorption energy, energy landscape, binding site, surface diffusion, molecular dynamics*

Interactions of gas molecules with metal surfaces and associated chemical reactions are critical in several subfields of chemistry. In heterogeneous catalysis, the knowledge of binding sites, binding strength, and surface mobility is helpful to understand reaction mechanisms and to make accurate predictions of reaction rates.[1−3] Likewise, in the corrosion of metals and alloys understanding oxygen interactions with metal surfaces is critical to predict mechanisms of oxidation, tailor corrosion-resistant materials, and mitigate annual damages of hundreds of billions of dollars.[4−6] Gas/metal interactions are also exploited in gas separations, such as pressure swing adsorption or temperature swing adsorption,[7,8] and in sensors with tailored surfaces and sorbents. Therefore, adsorption of gases has been studied extensively on many substrates,[2,9−11] including the structure and stability of adsorbed monolayers, multilayers, and coadsorption from gas mixtures.[12,13] Common measurements include changes in adsorbed mass, heat, spectroscopy and color, swelling, electrical properties, or chemical composition.[14−16]

However, a longstanding problem has been the unavailability of experimental and computational techniques to characterize adsorption and mobility of reactive gases such as molecular O_2 on metal and partially oxidized surfaces before and while the reactions take place, typically from femtoseconds to milliseconds (Figure 1).[17−20] In this study, we examined O_2 dynamics during this critical initial time window, an uncharted territory to-date, for pristine and partially oxidized metal surfaces. We identify correlations with reaction kinetics and products by comparison to experimental findings. To enable these insights, we have overcome limitations in computational techniques to simulate the dynamics of metal surfaces and gas molecules, achieving 10 to 50 times higher resolution and accuracy than previously possible by molecular dynamics (MD) and by density functional theory (DFT) simulations. We utilized XRD and LEED data for crystal structures before chemisorption and atomic arrangements after chemisorption to construct complete 3D potential energy surfaces, identify adsorption sites, and surface mobility (Figure 1).

Over the past decades, experimental studies have explored physical binding of O_2, N_2, CO, NO, rare gases, and other molecules to metal surfaces.[9,14,21,22] However, adsorbed states of O_2 are difficult to observe especially on Ni and Al surfaces, because O═O bond modification and oxide growth occur within seconds following adsorption, which is faster than calorimetry and many other macroscopic measurements.[23] Therefore, experiments using control of temperature and dosage of O_2 often only characterized the late stages of chemisorption and oxidation well.[24−26] At the same time, surface reconstruction, the location of chemisorbed oxygen atoms, and structures of oxide overlayers including on low index surfaces of Ni and Al[27,28] have been quantified by powerful techniques such as LEED,[29−33] SEXAFS,[32,34,35]

Received: April 9, 2022
Revised: June 16, 2022
Published: June 22, 2022

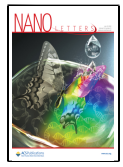

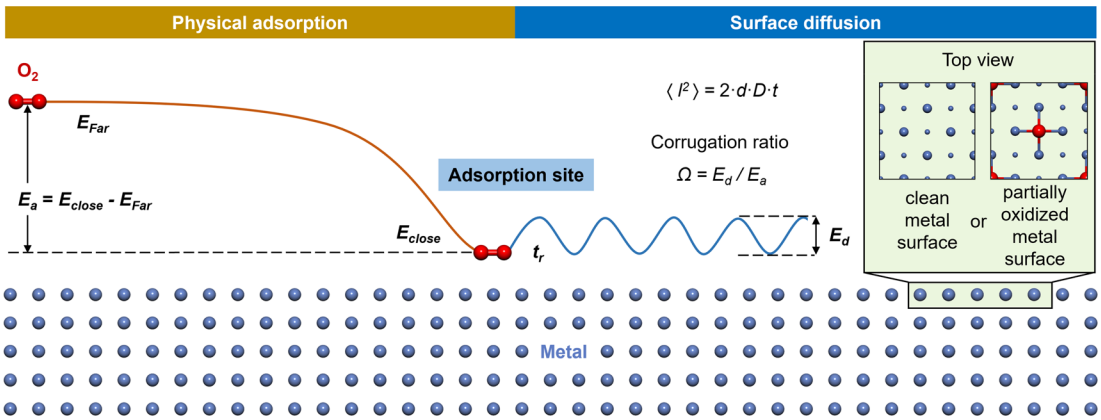

Figure 1. Schematic of adsorption and diffusion mechanisms on metal surfaces and partially oxidized metal surfaces. The interactions of O_2 with the surfaces are negligible at distances >12 Å and physical binding occurs as O_2 molecules approach the surfaces through random thermal motion or collisions with one another. We monitor the associated average energies, which equal E_{far} at large distance and E_{close} in equilibrium. Thereby, preferred adsorption sites on clean or partially oxidized surfaces (top view on the right) have the lowest energy E_{close} and the adsorption energy is given as $E_a = E_{close} - E_{far}$. The physically bound O_2 molecules can further diffuse on the surface, depending on the temperature, whereby the mean square displacement $\langle l^2 \rangle$ is proportional to the dimensionality of diffusion d (here typically $d = 2$), the diffusion constant D, and the elapsed time t. The molecules thereby overcome energy barriers of diffusion E_d specific to each (hkl) surface and the chosen diffusion path. For the most part, we focus on the minimum energy barrier for diffusion E_d on a given surface. The destiny of O_2 after travel on the surface on the nanosecond time scale is often desorption and return to the gas phase. The competition between diffusion and desorption of the molecule is characterized by the corrugation ratio (Ω), which equals the ratio between E_d (using the minimum value) and E_a.[56] Values of Ω much smaller than 1 indicate a preference for diffusion across the surface and values close to or greater than 1 indicate that desorption is preferred. The fractional residence time (t_r) measures the amount of time O_2 spends in close contact with the surfaces relative to the total time monitored. The top view on the right shows the clean and partially oxidized metal surfaces Ni (100) and Ni (100)-O-p2 × 2.

EELS,[36,37] and energy-dependent photodiffraction.[38] Changes in the electronic structure,[11,39−42] work functions,[43,44] surface vibrations,[45−47] and O_2 sticking probabilities[48] were also interrogated prior to complete oxidation to NiO or Al_2O_3, respectively.

In addition, quantum mechanical calculations have been widely used to fill gaps in understanding. However, model sizes are small, the computational footprint is too large to investigate dynamics, and results suggest instant changes in chemical bonding during picoseconds that contradict experimental observations of seconds. Moreover, computed surface energies of metals and gas adsorption energies with DFT often have over 50% uncertainty,[49,50] which limits correlations with experiments (see Section S1.1 in the Supporting Information for details).

As a result, the adsorption−desorption equilibria of O_2 on metals before O═O bond dissociation and reactions, which span at least 10^6 cycles from nanoseconds to milliseconds, are largely unexplored to-date.[3,15,24,51] We have no knowledge about the energy landscape of O_2 adsorption and dynamics on pure metals and on the partially oxidized surfaces that precede full oxidation. Neither experimental nor computational methods have so far been able to monitor these processes and quantitatively inform kinetic models of oxide growth.

In this Letter, we derive missing understanding in atomic detail. We analyzed the dynamics of O_2 molecules on 11 clean and partially oxidized Al and Ni (100), (110), and (111) surfaces using over 150 000 molecular mechanics (MM) and molecular dynamics (MD) simulations with the INTERFACE force field (IFF).[3,52−54] IFF matches lattice parameters of metals within 0.1%,[55] includes recent order-of-magnitude improved parameters for gases,[53] and reproduces surface energies of metals as well as gas-metal binding energies with only about 5% error relative to experiments.[3,53,55] Therefore, molecular simulations with IFF fill a gap in current methods by covering functionality unavailable in other force fields and by DFT methods, as well as high computational efficiency (see Section S1.1 in the Supporting Information for details).

We chose model surfaces that include six clean low-index surfaces (111), (100), and (110) of Ni and Al, as well as five representative partially oxidized surfaces (Ni (100)-O-p2 × 2, Ni (100)-O-c2 × 2, Ni (110)-O-c2 × 1, Ni (111)-O-p2 × 2, and Al (111)-O-p1 × 1), which were derived from experimental X-ray and LEED data (Figure 2, see details and references in Section S1.2 in the Supporting Information). Geometry optimizations and molecular dynamics simulations employed IFF parameters for metal surfaces[55] and O_2,[53] as well as specifically developed parameters for oxides and partially oxidized surfaces (Section S1.3, Tables S1 to S3, and Figure S1 in the Supporting Information).[52] These additions reproduce oxygen−metal bond distances and oxide geometries within 1%, as well as the interlayer spacing and layer buckling of the partially oxidized surfaces in agreement with LEED data (Section S1.4 and Figure S1 in the Supporting Information). We characterized preferred adsorption sites of O_2, molecular orientations, 3D potential energy landscapes, surface mobility, diffusion constants, and fractional residence times, all of which have been unknown to date (Figures 2−4 and Table 1).

Surface Geometry, O_2 Adsorption Sites, and Orientation. First, we analyzed the preferred oxygen adsorption sites, equilibrium distances, and molecular orientations on each surface using geometry optimization at 0 K (Figure 2 and Table 1). On the Ni (111), Ni (111)-O-p2 × 2, Al (111), and Al (111)-O-p1 × 1 surfaces, O_2 molecules adsorbed parallel to the long edge of the rectangular surface unit cell, whereby one O atom was located above a face-centered cubic (fcc) hollow site and the other O atom occupied an adjacent hollow site (Figure 2a−d). When such sites have limited availability as on the Ni (111)-O-p2 × 2 and Al (111)-O-p1 × 1 surfaces, the O atoms in O_2 aim for contact with epitaxial sites of nonoxidized

https://doi.org/10.1021/acs.nanolett.2c00490
Nano Lett. 2022, 22, 5392−5400

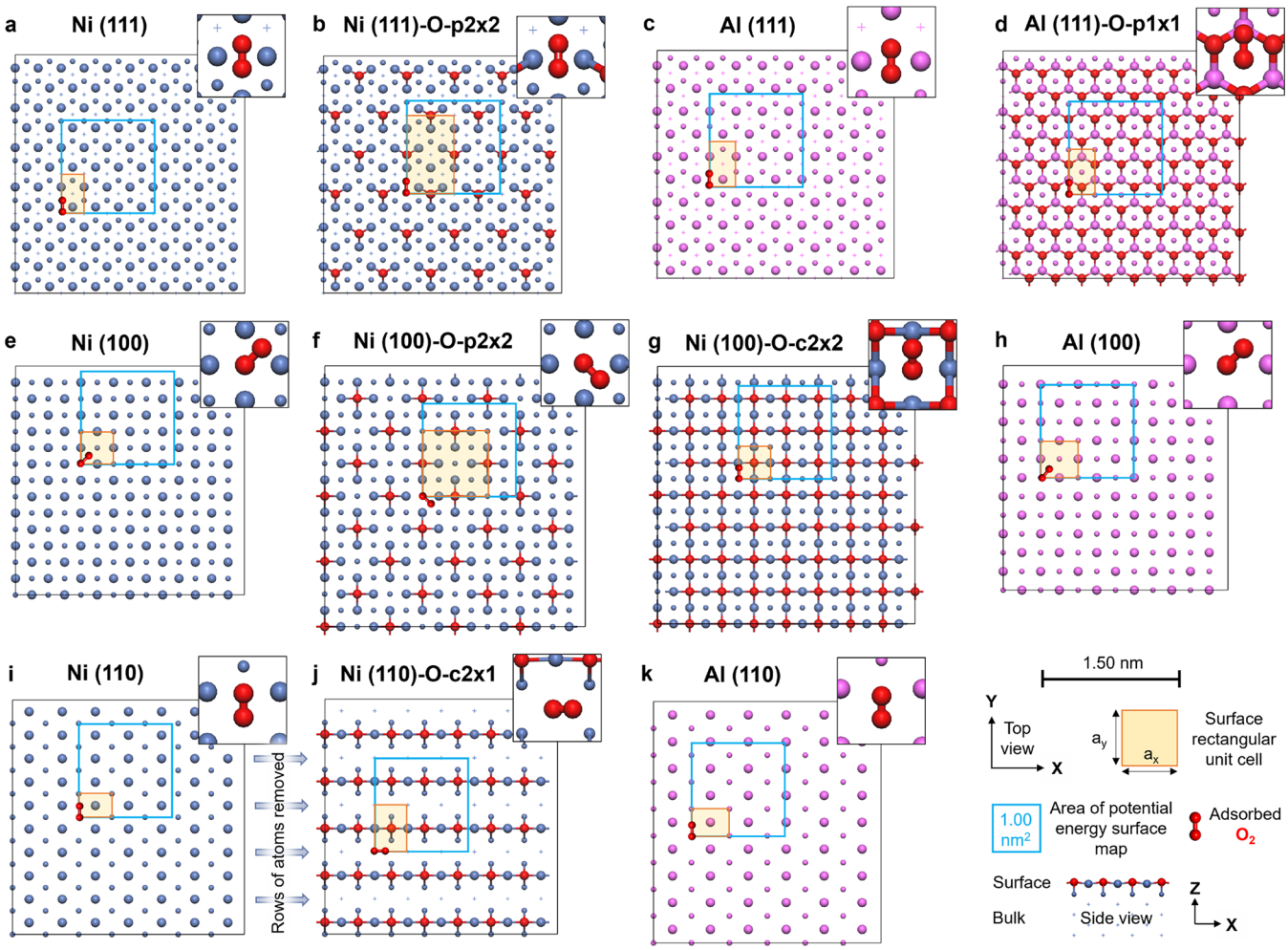

Figure 2. Structure of clean and partially oxidized (111), (100), and (110) surfaces of Ni and Al. Preferred adsorption sites of O_2 and orientations are shown, including magnified top views in the insets. (a) Clean Ni (111) surface, (b) oxidized Ni (111)-O-p2 × 2 surface, (c) clean Al (111) surface, (d) oxidized Al (111)-O-p1 × 1 surface, (e) clean Ni (100) surface, (f) Ni oxidized (100)-O-p2 × 2 surface, (g) oxidized Ni (100)-O-c2 × 2 surface, (h) clean Al (100) surface, (i) clean Ni (110) surface, (j) oxidized Ni (110)-O-c-2 × 1 surface, which involves major surface reconstruction relative to the Ni (110) surface upon partial oxidation, including removal of half of the rows of Ni surface atoms (see arrows),[66] and (k) clean Al (110) surface. The snapshots equal the 3D periodic boundaries of the simulation boxes. Yellow transparent boxes highlight rectangular surface unit cells, and blue boxes indicate a 1 × 1 nm^2 surface area used to generate 3D maps of the potential energy of O_2 adsorption in Figure 3. Top layer atoms are represented as large spheres, second layer atoms as smaller spheres, and atoms starting from the 3rd layer as crosses ("+" shape).

Ni or Al atoms in the remaining space between chemisorbed O atoms (Figure 2b,d). The adsorption mechanism and preferred orientation of O_2 agree with soft epitaxial adsorption previously observed for water molecules,[57,58] peptides,[59,60] and surfactants[61] in contact with metal surfaces.[54,62−65] Thus, soft epitaxial binding appears to be common for all types of molecules on metal surfaces, including gases, before chemical reactions occur.

On Ni (100), Ni (100)-O-p2 × 2, and Al (100) surfaces, oxygen molecules prefer orientations along the diagonal of the surface unit cell whereby one O atom is located above an epitaxial site and the other O atom points toward another epitaxial site (Figure 2e,g,h). As an exception, on the Ni (100)-O-c2 × 2 surface, the O_2 molecule adsorbs along a rectangular edge of the surface unit cell because adjacent diagonal epitaxial sites are occupied by chemisorbed O atoms (Figure 2f). The oxygen content on this Ni (100)-O-c2 × 2 surface atomic layer is twice as high ($NiO_{0.5}$) in comparison to the Ni (100)-O-p2 × 2 surface ($NiO_{0.25}$).

On the Ni (110), Ni (110)-O-c2 × 1, and Al (110) surfaces, O_2 molecules adsorb parallel to the short edge of the surface unit cell, whereby one O atom occupies a hollow site, and the other O atom is oriented toward another hollow site, aligned along a wide groove in these corrugated surfaces (Figure 2i−k).

The equilibrium distances from the surfaces (Table 1) and tilt angles of O_2 relative to the surface depend on the surface corrugation. Equilibrium tilt angles range from 0° to 34° (Figure S2 and discussion in Section S1.5 in the Supporting Information).

Three-Dimensional Energy Landscape of Oxygen Adsorption and Binding Energies. The potential energy landscape of O_2 adsorption on the clean and partially oxidized surfaces shows unique individual patterns (Figure 3). The relative energy of adsorption of oxygen molecules is shown in picometer resolution and in high accuracy of ±0.05 kcal/mol across a 1.00 × 1.00 nm^2 surface area. Energy differences characterize the barriers to move oxygen molecules across the

https://doi.org/10.1021/acs.nanolett.2c00490
Nano Lett. 2022, 22, 5392−5400

Table 1. Computed Adsorption and Diffusion Properties of O_2 in Contact with Pristine and Partially Oxidized Surfaces of Ni and Al before Chemical Reactions[a]

surface	equilibrium distance[b] (Å)	adsorption energy[c] E_a (kcal/mol)	diffusion barrier[d] E_d (kcal/mol)	corrugation ratio ($\lvert E_d/E_a \rvert$)	2D diffusion coefficient D (10^{-5} cm^2/s)			fractional residence time t_r (1.0 = 100%)[e]		
temp	0 K	0 K	0 K	0 K	298 K	423 K	573 K	298 K	423 K	573 K
(111) Clean and Chemisorbed Surfaces										
Ni	2.41	−9.98	0.38	0.038	107 ± 26	194 ± 20	386 ± 15	0.75	0.14	0.010
Ni−O-p2 × 2	1.30	−9.95	1.11	0.112	15 ± 3	45 ± 3	116 ± 4	0.40	0.022	0.0031
Al	2.54	−7.23	0.29	0.040	149 ± 18	275 ± 11	479 ± 11	0.18	0.012	0.0024
Al−O-p1 × 1	2.53	−6.24	0.20	0.032	170 ± 16	411 ± 15	662 ± 17	0.079	0.007	0.0017
(100) Clean and Chemisorbed Surfaces										
Ni	2.22	−9.45	0.29	0.031	57 ± 19	124 ± 11	259 ± 9	0.75	0.064	0.0068
Ni−O-p2 × 2	1.35	−10.61	1.05	0.099	16 ± 6	47 ± 3	128 ± 5	0.33	0.055	0.0067
Ni−O-c2 × 2	1.63	−7.91	1.60	0.202	19 ± 4	75 ± 5	186 ± 7	0.085	0.006	0.0015
Al	2.27	−7.14	0.20	0.028	51 ± 8	165 ± 6	332 ± 7	0.16	0.009	0.0019
(110) Clean and Chemisorbed Surfaces										
Ni	1.77	−10.5	0.37	0.035	12 ± 3	62 ± 9	154 ± 5	0.75	0.068	0.0069
Ni−O-c2 × 1	0.44	−11.2	2.05	0.183	5 ± 1	13 ± 2	110 ± 9	0.43	0.098	0.0073
Al	1.69	−8.2	0.24	0.029	30 ± 4	100 ± 4	221 ± 7	0.115	0.010	0.0022

[a]Equilibrium distances, adsorption energies, diffusion barriers, corrugation ratios, 2D diffusion coefficients, and fractional residence times are given. [b]The equilibrium distance was calculated as the difference in the z-coordinate from the topmost layer of metal surface atoms or chemisorbed O atom for partially oxidized surfaces to the nearest O atom in adsorbed O_2. The uncertainty is ±0.01 Å. [c]The adsorption energy corresponds to the energy difference upon approach of O_2 from vacuum (>12 Å) to the preferred adsorption site on the surface in minimum energy configuration. The uncertainty is ±0.1 kcal/mol. [d]Calculated from the path of minimum energy on the potential energy surface maps (Figure 3 and Figures S4 to S6 in the Supporting Information). The uncertainty is ±0.05 kcal/mol. [e]Average fractional residence time calculated from a 20 ns simulation trajectory including 6 O_2 molecules. The uncertainties in t_r are 20%, 10%, and 5% at 298, 423, and 573 K, respectively, of the values shown. At lower temperature, O_2 desorbs less frequently.

surface. Most favorable locations are shown in the darkest shade of blue (set as 0.00 kcal/mol) and least favorable locations in red, which reach up to +9.25 kcal/mol (Figure 3a−k). Adsorption energies are larger than this difference due to the extra energy needed for full detachment of O_2 from the surface by at least 12 Å (Table 1). The data assume a grid spacing of 0.05 Å and allow flexible orientation of one of the two O atoms in O_2, as well as flexibility of the z-coordinate of O_2 molecules (Figure S3 in the Supporting Information). For simplicity, we only consider the potential energy, that is, the total energy at a temperature of 0 K. Binding energies at 298 K and other temperatures follow the same trends and are reduced depending on the added kinetic energy (Table S4 in the Supporting Information).

The 3D potential energy landscapes help in explaining key aspects of O_2 adsorption, surface mobility, and the likely onset of oxidation reactions (Figure 4). Lowest energy barriers of diffusion E_d (Table 1) were derived from in-depth analysis of the enlarged images and their path profiles (Figures S4 to S6, as well as further details in Section S1.6 in the Supporting Information).

The adsorption energy, or binding energy, E_a characterizes the maximum strength of O_2 binding on the individual surfaces relative to desorption into vacuum (Figure 4a and Table 1). E_a ranges from −6 to −11 kcal/mol for all neat and oxidized Ni and Al. The binding affinity is higher to clean Ni surfaces than to the respective clean Al surfaces, which is a consequence of the higher surface energy of Ni compared to Al (2.24 vs 1.18 J/m^2).[55]

Among the three clean low-index surfaces, O_2 binds strongest to the (110) surfaces. Hollow (epitaxial) sites along vacant grooves are most favorable and sterically accessible binding sites (Figure 3i,k). The pristine (111) surfaces follow next in binding strength due to a good epitaxial match, and O_2 binds weakest to (100) surfaces.

Chemically bound oxygen atoms on the partially oxidized Ni (111) and Al (111) surfaces tend to decrease access of O_2 to the metal surface and lower the binding affinity by frequently deflecting incoming O_2 molecules away from the surface (Figure 4a, Table 1). In some instances, such as Ni (100)-O-p2 × 2 surfaces, a low area density of chemically bound O atoms can enhance surface interactions with O_2 while progressive oxidation, such as to Ni (100)-O-c2 × 2 surfaces, decreases O_2 adsorption due to less opportunity for contact with epitaxial sites of metallic Ni (Figure 4a, Figure 3f,g).

Two-Dimensional Diffusion Barriers, Diffusion Coefficients, and Residence Time of O_2. The 3D potential energy landscape indicates multiple diffusion paths of O_2 across the surface and associated energy barriers (Figure 3). We analyzed and compared the lowest energy barriers for diffusion E_d at 0 K, including full relaxation of all surface atoms (Figure 4b and Table 1). E_d ranges from 0.2 to 2.05 kcal/mol, which is clearly smaller than the corresponding adsorption energies E_a of −6 to −11 kcal/mol. Typical surface corrugation ratios Ω are therefore between 0.03 and 0.20 (Table 1). The clean (111) surfaces of Ni and Al have small activation energies for diffusion E_d of 0.38 and 0.29 kcal/mol, the (100) surfaces 0.29 and 0.20 kcal/mol, and the (110) surfaces 0.37 and 0.24 kcal/mol, respectively (Figure 4b and Table 1). Partial oxidation can lead to either increasing E_d to 1.1 to 1.6 kcal/mol on Ni or a decrease to 0.20 kcal/mol on Al surfaces.

The 2D diffusion coefficients D of the O_2 molecules on the surfaces describe the mobility and were calculated at three different temperatures of 298, 423, and 573 K (Figure 4c and Table 1). The values range from 10^{-5} to 10^{-2} cm^2/sec at room temperature and increase at higher temperature as expected due to more rapid thermal motion (Figure 4c). The order of

https://doi.org/10.1021/acs.nanolett.2c00490
Nano Lett. 2022, 22, 5392−5400

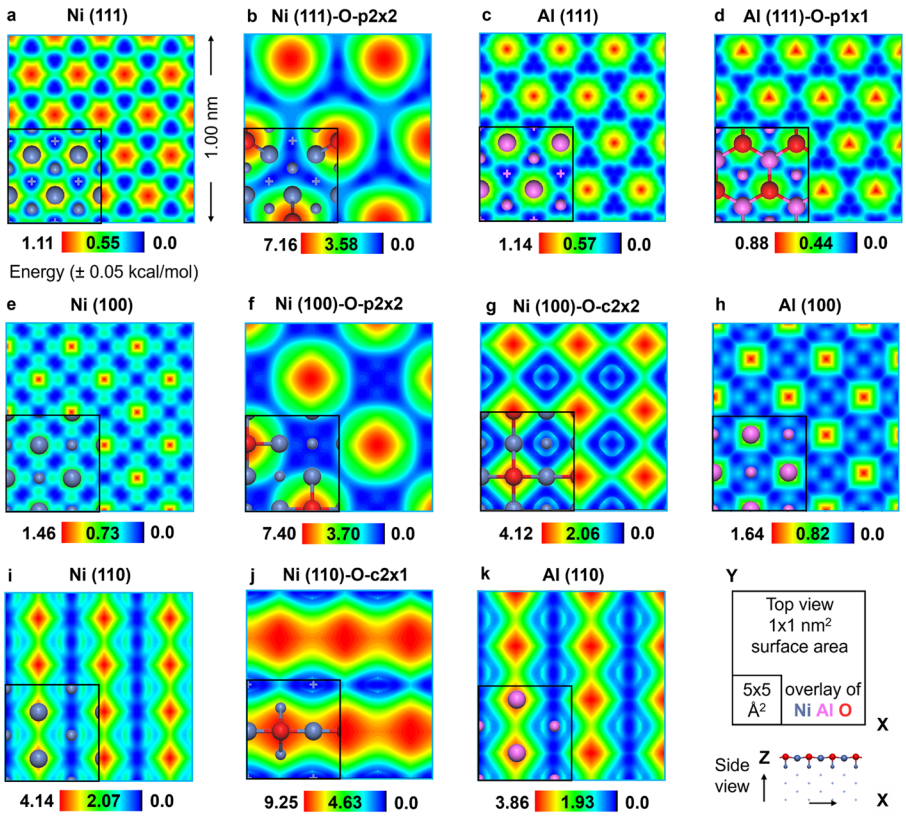

Figure 3. Three-dimensional potential energy landscape of adsorbed O_2 molecules. The interaction energies of oxygen molecules with the metal or partial metal oxide surfaces are shown for areas of 1.00 × 1.00 nm^2 size. (a) Ni (111), (b) Ni (111)-O-p2 × 2, (c) Al (111), (d) Al (111)-O-p1 × 1, (e) Ni (100), (f) Ni (100)-O-c2 × 2, (g) Ni (100)-O-p2 × 2, (h) Al (100), (i) Ni (110), (j) Ni (110)-O-c2 × 1, and (k) Al (110) surfaces. Blue-colored regions indicate areas of favorable low interaction energy and red colored regions show areas of unfavorable high interaction energy with O_2 on the surface. The maps are essential to understand the O_2 dynamics on the surfaces. The data were generated from ∼152 000 independent energy minimizations and the statistical uncertainty is ±0.05 kcal/mol.

magnitude is between the 3D self-diffusion coefficients of liquid water (1.90×10^{-5} cm^2/sec) and an order below that of air (1.98×10^{-1} cm^2/sec) at room temperature.[67] The sensitivity to temperature is surface-specific, for example, an increase to 573 K approximately triples the 2D diffusion constant on clean (111) surfaces, quintuples the value on clean (100) surfaces, and increases the diffusion constant about 10-fold on clean (110) surfaces (Figure 4c and Table 1). After partial oxidation, diffusion constants typically decrease due to stronger surface corrugation, higher energy barriers of diffusion, and more complex paths of motion.

The fractional residence time t_r decreased by up to 2 orders of magnitude on all surfaces as the temperature increased 298 to 573 K, ranging from 75% to 0.1% (Figure 4d and Table 1). O_2 spent more time on the clean Ni (hkl) surfaces with t_r of ∼75% than on the corresponding clean Al surfaces with a t_r of 11% to 18% at 298 K before desorption occurs, which is related to the higher surface energy of Ni and the associated increased "stickiness" E_a (Table 1). Upon partial oxidation, the residence time of O_2 decreased on all low index surfaces of Ni and Al to about half or less at 298 K (Figure 4d, Table 1). The residence time was also clearly lower on the more progressively oxidized Ni (100)-O-c2 × 2 surface compared to the less oxidized Ni (100)-O-p2 × 2 surface. O_2 molecules traveling across the surface also often collide with chemisorbed O atoms, which can change the momentum toward leaving the surface and reduces the residence time (Figure 4e). Such collisions do not occur on the clean surfaces where O_2 motion is less restricted in the horizontal plane (see details in Section S1.7 in the Supporting Information).

Impact of Surface Corrugation and Multiple Diffusion Paths on O_2 Mobility. O_2 mobility can be surprisingly affected by surface corrugation and multiple possible paths of surface diffusion. For example, binding of O_2 is stronger on the Ni (111)-O-p2 × 2 surface compared to the clean Ni (111) surface while the fractional residence time is lower on the Ni (111)-O-p2 × 2 surface (Table 1 and Figure 4a,d). Hereby, the presence of chemisorbed O atoms increases the surface roughness and collisions of these O atoms with O_2 molecules cause more frequent desorption of O_2 from the surface (Figure 4e). A similar, seemingly opposite trend in adsorption energy versus residence time was observed on the Ni (110)-O-c2 × 1 surface versus the clean Ni (110) surface at 298 K (Table 1, Figure 2i,j). In all cases, the relation between residence time t_r and the adsorption energy E_a can be expressed as a rate of desorption $\frac{1}{t_r} = Ae^{-E_a/RT}$ according to the Arrhenius equation. Hereby, surface corrugation by chemisorbed oxygen can change both the prefactor A (e.g., increase A) and the adsorption energy E_a (e.g., increase E_a).

Another less obvious trend is the relation between the computed minimum diffusion barrier E_d and the diffusion coefficient. The diffusion barrier is greater for the clean (111) surfaces when compared to the clean (100) surfaces (Table 1 and Figure 4b,c). However, opposite to expectations, O_2 diffuses faster on (111) surfaces and slower on (100) surfaces.

https://doi.org/10.1021/acs.nanolett.2c00490
Nano Lett. 2022, 22, 5392−5400

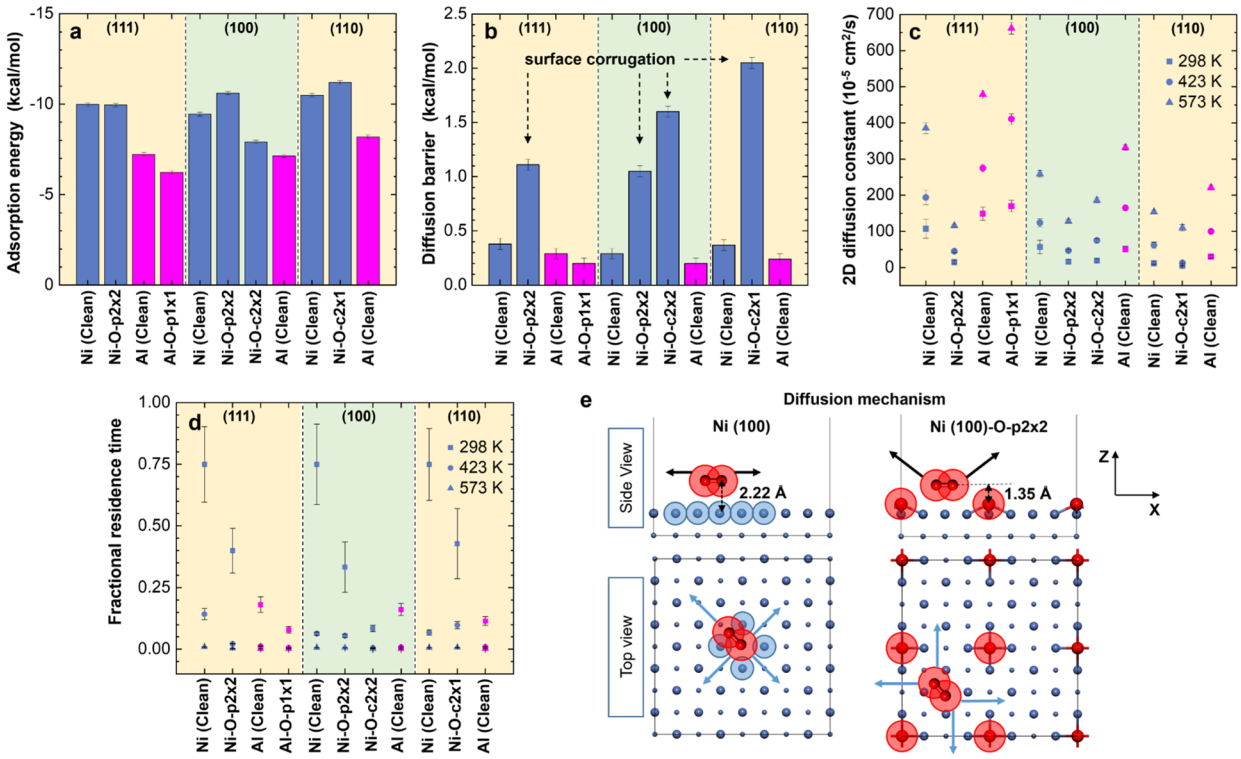

Figure 4. Adsorption energies and measures of O_2 mobility on clean and partially oxidized Ni and Al surfaces. (a) Adsorption energy (0 K), (b) lowest energy barrier for diffusion (0 K), (c) diffusion coefficient at different temperatures, and (d) fractional residence time at different temperatures. (e) Influence of surface oxidation on the diffusion mechanism. On a flat surface such as (100), the mobility of O_2 in the $x-y$ plane is high (left) while on corrugated, partially oxidized surfaces the mobility is sterically hindered by presence of chemisorbed O atoms (right). O_2 molecules then often collide with such "bumpy" atoms and desorb (black arrows on the right). The chemisorbed O atoms also have weaker interactions with O_2 molecules compared to Ni or Al. Blue arrows indicate diffusion paths of minimum resistance.

A similar trend was observed for Ni (100)-O-c2 × 2 and Ni (100)-O-p2 × 2 surfaces (Table 1 and Figure 4b,c). These relations originate from multiple paths of motion for O_2 from one adsorption site to another site, which include paths different from that of the minimum energy barriers E_d. It is therefore necessary to consider multiple diffusion barriers and associated mobilities, using the complete potential energy landscape, and not only the lowest barrier of diffusion E_d in Table 1.

Role of O_2 Adsorption in Metal Oxidation. Experiments have shown that reversible O_2 contact with clean and chemisorbed surfaces occurs many times before oxidation reactions or electrochemical conversions such as oxygen reduction reactions take place.[3,27,44] Physically bound states of O_2 were experimentally characterized on Pt (111)[14,21,22] with an adsorption energy of −8.5 ± 0.4 kcal/mol,[22] which matches the computed value with IFF of −8.0 ± 0.2 kcal/mol (free energy, −7.3 kcal/mol).[3] Available thermodynamic measurements of Xe adsorption on Ni (111) further indicate −8.5 kcal/mol (−369 meV)[9] and our computed adsorption energies for O_2 on clean and oxidized regions of Ni and Al surfaces are in a similar range (Table 1).

In comparison, DFT calculations exhibit ±70% uncertainty (Section 1.1 in the Supporting Information) and suggest O_2 dissociation and formation of covalent bonds within picoseconds, which contradicts the time scales of milliseconds to hours in experiments.[3,27,44] Therefore, energy landscapes from MD simulations provide reliable understanding of the initial O_2 dynamics that leads to the formation of chemisorbed oxygen, enabling quantitative hypotheses for the nucleation and growth of oxide domains in conjunction with LEED data and ab initio studies at the local scale (Figure 2b,d,f,g,j).[27,28] The 2D diffusion coefficients can also be utilized in models to predict nucleation and growth rates of oxide islands up to the macroscopic scale (Table 1 and further discussion in Section S1.8 of the Supporting Information).[24]

Correlation of O_2 Adsorption with Oxidation Rates and Catalyst Performance. The results correlate with the relative initial reaction rates of O_2 with Ni surfaces observed in experiments, which decrease in the order Ni (110) > Ni (111) > Ni (100).[68] Oxidation is fastest for the Ni (110) surface where the computed binding energy of O_2 is largest at −10.5 kcal/mol, followed by −10.0 and −9.5 kcal/mol on (111) and (100) surfaces, respectively (Figure 4a). The coordination number of O_2 with Ni decreases in the same order. The O_2−Ni coordination number is highest when adsorbed in the concave grooves on Ni (110) surfaces, is reduced on the flat (111) surface, and is lowest on the wider spaced (100) surface of square geometry (Figure 2a,e,i). Accordingly, there is statistically decreasing contact opportunity of O_2 with Ni (110) > Ni (111) > Ni (100) surfaces for initial electron transfer and formation of NiO oxide layers during the incubation period of milliseconds to seconds. The rate of electron transfer is likely similar for Ni atoms on different Ni (hkl) surfaces, as previously noted for Pt surfaces,[3] and the adsorption energy of O_2 can be used as a measure for surface contact time to estimate the relative rate of oxidation of differently structured Ni surfaces.

The methods can also be employed to investigate reactions in catalytic converters (see details in Section S1.9 in the

https://doi.org/10.1021/acs.nanolett.2c00490
Nano Lett. 2022, 22, 5392−5400

Supporting Information).[1,69] Energy landscapes of reactant adsorption and temperature-dependent diffusion likely affect and sometimes determine the outcomes of reactions. The analysis of binding sites, molecular orientations, adsorption energies, and selectivities (in gas mixtures) can provide promising descriptors for reaction pathways and rates in combination with experiments. MD simulations with IFF can include the role of defects, changes in bonding during reactions, and time scales up to microseconds and can provide high quality inputs for QM and QM/MM analysis on the local scale.[3,54]

■ ASSOCIATED CONTENT

Supporting Information

The Supporting Information is available free of charge at https://pubs.acs.org/doi/10.1021/acs.nanolett.2c00490.

Supporting figures and tables with details of surface reconstruction, 3D visualizations of oxygen binding, computation of energy profiles, force field parameters, temperature effects on adsorption, unit cells parameters, thermal expansion; supporting text including comparisons of earlier methods and additional descriptions of results, details of methods, opportunities, and limitations (PDF)

Highlights of O_2 binding and diffusion mechanisms on clean and partially oxidized Ni(110) surfaces as seen in molecular dynamics simulation (MP4)

Supporting data files, force field files, and simulation scripts to reproduce the results and study related problems (ZIP)

■ AUTHOR INFORMATION

Corresponding Author

Hendrik Heinz − *Department of Chemical and Biological Engineering, University of Colorado at Boulder, Boulder, Colorado 80309, United States;* orcid.org/0000-0002-6776-7404; Email: hendrik.heinz@colorado.edu

Author

Krishan Kanhaiya − *Department of Chemical and Biological Engineering, University of Colorado at Boulder, Boulder, Colorado 80309, United States;* orcid.org/0000-0002-3622-2655

Complete contact information is available at: https://pubs.acs.org/10.1021/acs.nanolett.2c00490

Author Contributions

K.K. designed the study, performed the simulations, collected the data, analyzed the data, and wrote the manuscript. H.H. designed the study, analyzed the data, and wrote the manuscript.

Notes

The authors declare no competing financial interest.

■ ACKNOWLEDGMENTS

This work was supported by the National Science Foundation (DMREF 1623947, OAC 1931587, CMMI 1940335) and the Office of Naval Research (ONR-MURI-N00014-14-1-0675). The allocation of computational resources is acknowledged at the Argonne Leadership Computing Facility, which is a DOE Office of Science User Facility supported under contract DE-AC02-06CH11357, and at the Summit supercomputer supported by the National Science Foundation (award number ACI-1532235 and ACI-1532236). We thank Alfaia BaSallom for assistance with the computations.

■ REFERENCES

(1) Ma, Z.; Zaera, F. Heterogeneous Catalysis by Metals. In *Encyclopedia of Inorganic and Bioinorganic Chemistry*; Scott, R. A., Ed.; John Wiley & Sons, Ltd: Chichester, 2014.

(2) Liu, L.; Corma, A. Metal Catalysts for Heterogeneous Catalysis: from Single Atoms to Nanoclusters and Nanoparticles. *Chem. Rev.* **2018**, *118*, 4981−5079.

(3) Wang, S.; Zhu, E.; Huang, Y.; Heinz, H. Direct Correlation of Oxygen Adsorption on Platinum-Electrolyte Interfaces with the Activity in the Oxygen Reduction Reaction. *Sci. Adv.* **2021**, *7*, eabb1435.

(4) Koch, G. Cost of Corrosion. In *Trends in Oil and Gas Corrosion Research and Technology*; El-Sherik, A. M., Ed.; Elsevier, 2017; pp 3−30.

(5) Koch, G. H.; Brongers, M. P. H.; Thompson, N. G.; Virmani, Y. P.; Payer, J. H. Cost of Corrosion in the United States. In *Handbook of Environmental Degradation of Materials*; Kutz, M., Ed.; Elsevier, 2005; pp 3−24.

(6) Hou, B.; Li, X.; Ma, X.; Du, C.; Zhang, D.; Zheng, M.; Xu, W.; Lu, D.; Ma, F. The Cost of Corrosion in China. *npj Mater. Degrad.* **2017**, *1*, 1−10.

(7) Grande, C. A. Advances in Pressure Swing Adsorption for Gas Separation. *Int. Scholarly Res. Not.* **2012**, *2012*, 982934.

(8) Yang, R.; Doong, S. Gas Separation by Pressure Swing Adsorption: A Pore-Diffusion Model for Bulk Separation. *AIChE J.* **1985**, *31*, 1829−1842.

(9) Vidali, G.; Ihm, G.; Kim, H.-Y.; Cole, M. W. Potentials of Physical Adsorption. *Surf. Sci. Rep.* **1991**, *12*, 135−181.

(10) Shamim, T.; Shen, H.; Sengupta, S.; Son, S.; Adamczyk, A. A Comprehensive Model to Predict Three-Way Catalytic Converter Performance. *J. Eng. Gas Turbines Power* **2002**, *124*, 421−428.

(11) Das, N. K.; Shoji, T. Early Stage Oxidation of Ni−Cr Binary Alloy (111), (110) and (100) Surfaces: A Combined Density Functional and Quantum Chemical Molecular Dynamics Study. *Corros. Sci.* **2013**, *73*, 18−31.

(12) Ivanova, E.; Mihaylov, M.; Thibault-Starzyk, F.; Daturi, M.; Hadjiivanov, K. FTIR spectroscopy study of CO and NO Adsorption and Co-Adsorption on Pt/TiO_2. *J. Mol. Catal. A: Chem.* **2007**, *274*, 179−184.

(13) Rioux, R. M.; Hoefelmeyer, J. D.; Grass, M.; Song, H.; Niesz, K.; Yang, P.; Somorjai, G. A. Adsorption and Co-adsorption of Ethylene and Carbon Monoxide on Silica-Supported Monodisperse Pt Nanoparticles: Volumetric Adsorption and Infrared Spectroscopy Studies. *Langmuir* **2008**, *24*, 198−207.

(14) Wartnaby, C.; Stuck, A.; Yeo, Y.; King, D. Microcalorimetric Heats of Adsorption for CO, NO, and Oxygen on Pt {110}. *J. Phys. Chem.* **1996**, *100*, 12483−12488.

(15) Shayegan, M.; Cavallo, J.; Glover, R., III; Park, R. L. Precursor Adsorption of Oxygen on Ni (111) and the Activation Energy for Chemisorption. *Phys. Rev. Lett.* **1984**, *53*, 1578.

(16) Comini, E. Metal Oxide Nano-Crystals for Gas Sensing. *Anal. Chim. Acta* **2006**, *568*, 28−40.

(17) Uhlig, H.; Pickett, J.; MacNairn, J. Initial Oxidation Rate of Nickel and Effect of the Curie Temperature. *Acta Metall.* **1959**, *7*, 111−117.

(18) Rai, A.; Park, K.; Zhou, L.; Zachariah, M. Understanding the Mechanism of Aluminium Nanoparticle Oxidation. *Combust. Theory Modell.* **2006**, *10*, 843−859.

(19) Zhou, G.; Yang, J. C. Initial Oxidation Kinetics of Copper (1 1 0) Film Investigated by In Situ UHV-TEM. *Surf. Sci.* **2003**, *531*, 359−367.

(20) Krueger, W. H.; Pollack, S. The Initial Oxidation of Aluminum Thin Films at Room Temperature. *Surf. Sci.* **1972**, *30*, 263−279.

(21) Montemore, M. M.; van Spronsen, M. A.; Madix, R. J.; Friend, C. M. O_2 Activation by Metal Surfaces: Implications for Bonding and Reactivity on Heterogeneous Catalysts. *Chem. Rev.* **2018**, *118*, 2816−2862.
(22) Gland, J. L.; Sexton, B. A.; Fisher, G. B. Oxygen Interactions with the Pt(111) Surface. *Surf. Sci.* **1980**, *95*, 587−602.
(23) Vattuone, L.; Yeo, Y. Y.; King, D. A. Adatom Bond Energies and Lateral Interaction Energies from Calorimetry: NO, O_2, and N_2 adsorption on Ni{100}. *J. Chem. Phys.* **1996**, *104*, 8096−8102.
(24) Holloway, P. H.; Hudson, J. B. Kinetics of the Reaction of Oxygen with Clean Nickel Single Crystal Surfaces: I. Ni(100) Surface. *Surf. Sci.* **1974**, *43*, 123−140.
(25) Michel, R.; Gastaldi, J.; Allasia, C.; Jourdan, C.; Derrien, J. Initial Interaction of Oxygen with Aluminium Single Crystal Faces: A LEED, AES and Work Function Study. *Surf. Sci.* **1980**, *95*, 309−320.
(26) Kortan, A. R.; Park, R. L. Phase Diagram of Oxygen Chemisorbed on Nickel (111). *Phys. Rev. B* **1981**, *23*, 6340−6347.
(27) Besenbacher, F.; Nørskov, J. K. Oxygen Chemisorption on Metal Surfaces: General Trends for Cu, Ni and Ag. *Prog. Surf. Sci.* **1993**, *44*, 5−66.
(28) Batra, I. P.; Kleinman, L. Chemisorption of Oxygen on Aluminum Surfaces. *J. Electron Spectrosc. Relat. Phenom.* **1984**, *33*, 175−241.
(29) Marcus, P. M.; Demuth, J. E.; Jepsen, D. W. Determination of the Structure of Ordered Adsorbed Layers by Analysis of LEED Spectra. *Surf. Sci.* **1975**, *53*, 501−522.
(30) Onuferko, J. H.; Woodruff, D. P.; Holland, B. W. Leed Structure Analysis of the Ni{100} (2 × 2)C (p4g) Structure; A Case of Adsorbate-Induced Substrate Distortion. *Surf. Sci.* **1979**, *87*, 357−374.
(31) Englert, W.; Heiland, W.; Taglauer, E.; Menzel, D. The Sorption of CO and O on Ni (111) Studied by Leed and ISS. *Surf. Sci.* **1979**, *83*, 243−252.
(32) Wenzel, L.; Arvanitis, D.; Daum, W.; Rotermund, H. H.; Stöhr, J.; Baberschke, K.; Ibach, H. Structural Determination of an Adsorbate-Induced Surface Reconstruction: p4g(2 × 2)N versus c(2 × 2)O on Ni(100). *Phys. Rev. B* **1987**, *36*, 7689−7692.
(33) Burchhardt, J.; Nielsen, M. M.; Adams, D. L.; Lundgren, E.; Andersen, J. N. Structure of Al(111)-($\sqrt{3} \times \sqrt{3}$)R30°-Na: A LEED study. *Phys. Rev. B* **1994**, *50*, 4718−4724.
(34) Johansson, L. I.; Stöhr, J. Bonding of Oxygen on Al(111): A Surface Extended X-Ray Absorption Fine-Structure Study. *Phys. Rev. Lett.* **1979**, *43*, 1882−1885.
(35) Stöhr, J.; Johansson, L. I.; Brennan, S.; Hecht, M.; Miller, J. N. Surface Extended-X-Ray-Absorption-Fine-Structure Study of Oxygen Interaction with Al(111) Surfaces. *Phys. Rev. B* **1980**, *22*, 4052−4065.
(36) De Crescenzi, M.; Antonangeli, F.; Bellini, C.; Rosei, R. Surface Extended Energy-Loss Fine Structures of Oxygen on Ni(100). *Phys. Rev. Lett.* **1983**, *50*, 1949−1952.
(37) Caputi, L. S.; Jiang, S. L.; Amoddeo, A.; Tucci, R. Oxygen-Nickel Bond Length in Ni(111)-p(2 × 2)O Determined by Electron-Energy-Loss Fine-Structure Spectroscopy. *Phys. Rev. B* **1990**, *41*, 8513−8515.
(38) Tong, S.; Kang, W.; Rosenblatt, D.; Tobin, J.; Shirley, D. Photoelectron-diffraction Analysis of the Structure of c (2× 2) O on Ni (001). *Phys. Rev. B* **1983**, *27*, 4632−4632.
(39) Altmann, W.; Desinger, K.; Donath, M.; Dose, V.; Goldmann, A.; Scheidt, H. Dispersion of an Empty Adsorbate Band — The p(2 × 2) Oxygen Overlayer on Ni(111). *Surf. Sci. Lett.* **1985**, *151*, L185−L190.
(40) Eastman, D. E.; Cashion, J. K. Photoemission Energy-Level Measurements of Chemisorbed CO and O on Ni. *Phys. Rev. Lett.* **1971**, *27*, 1520−1523.
(41) Desinger, K.; Dose, V.; Goldmann, A.; Jacob, W.; Scheidt, H. Inverse Photoemission Studies of Oxygen on Ni(110) and Ni(100). *Surf. Sci.* **1985**, *154*, 695−703.
(42) Flodstrom, S. A.; Bachrach, R. Z.; Bauer, R. S.; Hagström, S. B. M. Multiple Oxidation States of Al Observed by Photoelectron Spectroscopy of Substrate Core Level Shifts. *Phys. Rev. Lett.* **1976**, *37*, 1282−1285.
(43) Mac Rae, A. U. Adsorption of Oxygen on the {111}, {100} and {110} Surfaces of Clean Nickel. *Surf. Sci.* **1964**, *1*, 319−348.
(44) Gartland, P. O. Adsorption of Oxygen on Clean Single Crystal Faces of Aluminium. *Surf. Sci.* **1977**, *62*, 183−196.
(45) Voigtländer, B.; Lehwald, S.; Ibach, H. Symmetry and Structure of the Reconstructed Ni(110)-(2 × 1)O Surface. *Surf. Sci.* **1990**, *225*, 162−170.
(46) Rahman, T. S.; Mills, D. L.; Black, J. E.; Szeftel, J. M.; Lehwald, S.; Ibach, H. Surface Phonons and the c(2 × 2) Oxygen Overlayer on Ni(100): Theory and Experiment. *Phys. Rev. B* **1984**, *30*, 589−603.
(47) Ibach, H.; Bruchmann, D. Observation of Surface Phonons on Ni(111) by Electron Energy-Loss Spectroscopy. *Phys. Rev. Lett.* **1980**, *44*, 36−39.
(48) Stuckless, J. T.; Wartnaby, C. E.; Al-Sarraf, N.; Dixon-Warren, S. J. B.; Kovar, M.; King, D. A. Oxygen Chemisorption and Oxide Film Growth on Ni{100}, {110}, and {111}: Sticking Probabilities and Microcalorimetric Adsorption Heats. *J. Chem. Phys.* **1997**, *106*, 2012−2030.
(49) Singh-Miller, N. E.; Marzari, N. Surface Energies, Work Functions, and Surface Relaxations of Low-Index Metallic Surfaces From First Principles. *Phys. Rev. B* **2009**, *80*, 235407.
(50) Ruiz, V. G.; Liu, W.; Tkatchenko, A. Density-Functional Theory with Screened van der Waals Interactions Applied to Atomic and Molecular Adsorbates on Close-Packed and Non-Close-Packed Surfaces. *Phys. Rev. B* **2016**, *93*, 035118.
(51) Panas, I.; Siegbahn, P.; Wahlgren, U. The Mechanism for the O_2 Dissociation on Ni(100). *J. Chem. Phys.* **1989**, *90*, 6791−6801.
(52) Heinz, H.; Lin, T.-J.; Mishra, R. K.; Emami, F. S. Thermodynamically Consistent Force Fields for the Assembly of Inorganic, Organic, and Biological Nanostructures: The INTERFACE Force Field. *Langmuir* **2013**, *29*, 1754−1765.
(53) Wang, S.; Hou, K.; Heinz, H. Accurate and Compatible Force Fields for Molecular Oxygen, Nitrogen, and Hydrogen to Simulate Gases, Electrolytes, and Heterogeneous Interfaces. *J. Chem. Theory Comput.* **2021**, *17*, 5198−5213.
(54) Mark, L. O.; Zhu, C.; Medlin, J. W.; Heinz, H. Understanding the Surface Reactivity of Ligand-Protected Metal Nanoparticles for Biomass Upgrading. *ACS Catal.* **2020**, *10*, 5462−5474.
(55) Heinz, H.; Vaia, R. A.; Farmer, B. L.; Naik, R. R. Accurate Simulation of Surfaces and Interfaces of Face-Centered Cubic Metals Using 12−6 and 9−6 Lennard-Jones Potentials. *J. Phys. Chem. C* **2008**, *112*, 17281−17290.
(56) Brand, J.; Arena, M.; Deckert, A.; George, S. Surface Diffusion of n-Alkanes on Ru (001). *J. Chem. Phys.* **1990**, *92*, 5136−5143.
(57) Geada, I. L.; Ramezani-Dakhel, H.; Jamil, T.; Sulpizi, M.; Heinz, H. Insight into Induced Charges at Metal Surfaces and Biointerfaces Using a Polarizable Lennard-Jones Potential. *Nat. Commun.* **2018**, *9*, 716.
(58) Ramezani-Dakhel, H.; Ruan, L. Y.; Huang, Y.; Heinz, H. Molecular Mechanism of Specific Recognition of Cubic Pt Nanocrystals by Peptides and the Concentration-Dependent Formation from Seed Crystals. *Adv. Funct. Mater.* **2015**, *25*, 1374−1384.
(59) Heinz, H.; Farmer, B. L.; Pandey, R. B.; Slocik, J. M.; Patnaik, S. S.; Pachter, R.; Naik, R. R. Nature of Molecular Interactions of Peptides with Gold, Palladium, and Pd-Au Bimetal Surfaces in Aqueous Solution. *J. Am. Chem. Soc.* **2009**, *131*, 9704−9714.
(60) Ramezani-Dakhel, H.; Bedford, N. M.; Woehl, T. J.; Knecht, M. R.; Naik, R. R.; Heinz, H. Nature of Peptide Wrapping onto Metal Nanoparticle Catalysts and Driving Forces for Size Control. *Nanoscale* **2017**, *9*, 8401−8409.
(61) Feng, J.; Pandey, R. B.; Berry, R. J.; Farmer, B. L.; Naik, R. R.; Heinz, H. Adsorption Mechanism of Single Amino Acid and Surfactant Molecules to Au {111} Surfaces in Aqueous Solution: Design Rules for Metal-Binding Molecules. *Soft Matter* **2011**, *7*, 2113−2120.
(62) Ruan, L.; Ramezani-Dakhel, H.; Chiu, C.-Y.; Zhu, E.; Li, Y.; Heinz, H.; Huang, Y. Tailoring Molecular Specificity Toward a

Crystal Facet: A Lesson From Biorecognition Toward Pt{111}. *Nano Lett.* **2013**, *13*, 840−846.
(63) Firment, L. E.; Somorjai, G. A. Surface Structures of Normal Paraffins and Cyclohexane Monolayers and Thin Crystals Grown on the (111) Crystal Face of Platinum. A Low-Energy Electron Diffraction Study. *J. Chem. Phys.* **1977**, *66*, 2901−2913.
(64) Atanasoska, L. L.; Buchholz, J. C.; Somorjai, G. A. Low-Energy Electron Diffraction Study of the Surface Structures of Adsorbed Amino Acid Monolayers and Ordered Films Deposited on Copper Crystal Surfaces. *Surf. Sci.* **1978**, *72*, 189−207.
(65) Heinz, H.; Ramezani-Dakhel, H. Simulations of Inorganic−Bioorganic Interfaces to Discover New Materials: Insights, Comparisons to Experiment, Challenges, and Opportunities. *Chem. Soc. Rev.* **2016**, *45*, 412−448.
(66) Kleinle, G.; Wintterlin, J.; Ertl, G.; Behm, R. J.; Jona, F.; Moritz, W. Reconstruction and Subsurface Lattice Distortions in the (2 × 1)O-Ni(110) Structure: A LEED Analysis. *Surf. Sci.* **1990**, *225*, 171−183.
(67) Schmitz, D.; Anlauf, R.; Rehrmann, P. Effect of Air Content on the Oxygen Diffusion Coefficient of Growing Media. *Am. J. Plant Sci.* **2013**, *4*, 955−963.
(68) Norton, P.; Tapping, R.; Goodale, J. A Photoemission Study of the Interaction of Ni (100),(110) and (111) Surfaces with Oxygen. *Surf. Sci.* **1977**, *65*, 13−36.
(69) Chatterjee, D.; Deutschmann, O.; Warnatz, J. Detailed Surface Reaction Mechanism in a Three-Way Catalyst. *Faraday Discuss.* **2001**, *119*, 371−384.

https://doi.org/10.1021/acs.nanolett.2c00490
Nano Lett. 2022, 22, 5392−5400